4 A METHOD TO DETECT TRIPLET EXCITON TRANSFER FROM SINGLET FISSION INTO SILICON SOLAR CELLS: COMPARING DIFFERENT SURFACE TREATMENTS

This chapter is based on the following publication:

Benjamin Daiber, Sidharam P Pujari, Steven Verboom, Stefan L Luxembourg, Stefan W Tabernig, Moritz H Futscher, Jumin Lee, Han Zuilhof, and Bruno Ehrler. "A Method to Detect Triplet Exciton Transfer from Singlet Fission Materials into Silicon Solar Cells: Comparing Different Surface Treatments" In: *The Journal of Chemical Physics* (2020)

Singlet fission is one of the most promising routes to overcoming the single-junction efficiency limit for solar cells. Singlet fission-enhanced silicon solar cells are the most desirable implementation, but transfer of triplet excitons, the product of singlet fission, into silicon solar cells has proved very challenging. Here we report on an all optical measurement technique for the detection of triplet exciton quenching at semiconductor interfaces, a necessary requirement for triplet exciton or charge transfer. The method relies on growth of individual, single-crystal islands of the singlet fission material on the silicon surface. The islands have different heights, and we correlate these heights to the quenching efficiency of triplet excitons. The quenching efficiency is measured by spatially-

resolved delayed fluorescence and compared to a diffusion-quenching model. Using silicon capped with a blocking thermal oxide and aromatic monolayers, we demonstrate that this technique can quickly screen different silicon surface treatments for triplet exciton quenching.

4.1 INTRODUCTION

The efficiency of silicon solar cells is already very close to its theoretical limit [99], which drives the search for new concepts to increase power conversion efficiency. Next to tandem solar cells, singlet fission has emerged as a promising route to allow for higher efficiency [47], with comparably simple implementation in solar cell devices, and spectral stability in changing environmental conditions [34].

Singlet fission is the conversion of one singlet exciton in an organic semiconductor into two triplet excitons of roughly half the energy [100, 118]. Triplet excitons are dark states that cannot transfer energy radiatively or *via* a Förster type process, only Dexter type transfer or charge disassociation and subsequent charge transfer is possible. For an increase in power conversion efficiency these triplet excitons need to be transferred into a lower-bandgap semiconductor cell to generate additional current. One implementation where singlet fission enhances the current of a silicon solar cell (in a narrow spectral range) relies on a tandem cell configuration. Two separate cells are optically connected in series and electrically connected in parallel [69, 91]. Fabrication of these tandem solar cells would be equally as involved as conventional tandem solar cells. It would be more elegant to directly transfer triplet excitons into silicon which would not require any changes to the contacts of a conventional silicon solar cell.

In contrast, if the triplet excitons could be directly transferred into the low-bandgap semiconductor via charge or energy transfer, a very simple device implementation would be possible. Such transfer has successfully been shown for purely organic solar cells [68], into quantum dots [28, 125, 129], and silicon using a hafnium oxynitride (HfO_xN_y) interlayer [29]. In

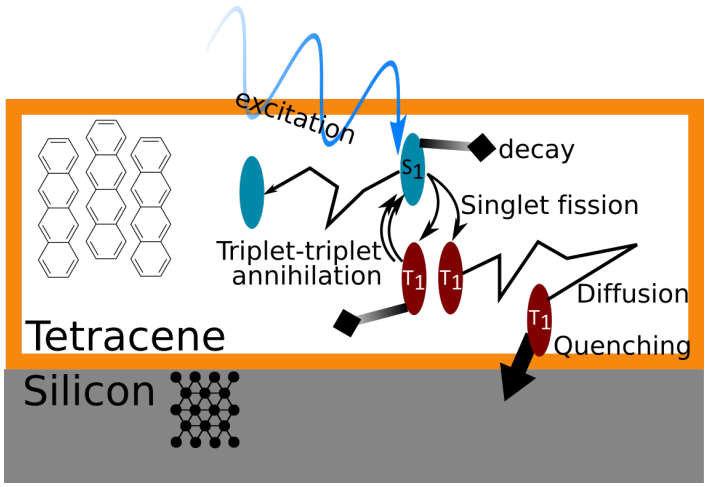

Figure 4.1: Schematics of the processes included in the simulation. Excitation with a short laser pulse is followed by singlet fission in tetracene and diffusion of both singlet and triplet excitons. Singlet and triplet excitons have various non-radiative decay mechanisms that can be summarized with one decay rate. Quenching at the interface is assumed to be only present for triplets. The simulations allow us to calculate the density of singlet and triplet excitons over time. The singlet exciton density is proportional to the emitted photons, which is the observable in our experiment.

the last example, a single layer of singlet fission material on top of the silicon cell absorbs the high-energy part of the spectrum, generates up to two triplet excitons per photon, and injects the energy of the excitons into silicon with an, as of yet, unspecified pathway; the injection has to proceed either via direct Dexter energy transfer [24], where both the electron and hole are concurrently transferred into silicon, or the transfer of a single charge at the heterojunction interface. Dexter transfer is observed for triplet transfer from pentacene into PbSe quantum dots [125], from tetracene into PbS quantum dots [129] and from tetracene into silicon [29]. Charge transfer has been observed at multiple organic/organic interfaces [17, 144], at the organic/quantum dot interface [27, 53, 145] at the organic/a-Si interface with a quantum dot interlayer [26]. Several attempts to show direct transfer of excitons or charges into crystalline silicon remained unsuccessful or inconclusive [76, 95], and only recently current enhancement of a silicon solar cell using a HfO_xN_y interlayer between tetracene and silicon has been demonstrated [29].

One major hurdle in the path towards the triplet exciton transfer into silicon is the detection method of such transfer. Triplet excitons are "dark states", meaning that they do not emit or absorb light in the absence of strong spin-orbit coupling. The only direct optical measurement is therefore transient absorption spectroscopy, which has been employed to measure the charge separation dynamics at the pentacene/C_{60} interface [105]. Transient absorption at the silicon interface is considerably more challenging because the features in silicon are comparably unspecific, and the absorption in the silicon solar cell reduces the signal. Further, spatially resolved studies are even more difficult [143], and excitation densities are typically orders of magnitude above those relevant in solar cells which makes it difficult to draw conclusions from these studies for solar cell operation.

A popular method to detect the contribution of triplet excitons to the photocurrent of a solar cells is to measure the photocurrent as a function of an externally applied magnetic field [144]. The field changes the ratio of singlet excitons to triplet excitons generated from photons absorbed in the singlet fission materials. At high external fields (100 mT), the ratio of singlets to triplets increases [79]. Thus, the photocurrent contribution

from triplets decreases. This method is very accurate, but it requires fabricating a solar cell, and the magnetic field measurement on a full solar cell device requires careful separation of magnetic field effects from the singlet fission contribution and form other layers in the solar cell stack. It is also a measurement that is typically done on bulk films which means that each variation in the materials parameters requires the fabrication of a separate solar cell.

Similarly, to the magnetic field measurement of the photocurrent of a solar cell, one can use the photoluminescence of the low bandgap semiconductor as an indication for energy transfer. If excitons are injected into silicon, then the photoluminescence (PL) of silicon can be used to measure triplet and singlet exciton injection [29]. The change of PL with magnetic field allows one to distinguish between triplet and singlet exciton injection. However, for example for silicon the photoluminescence quantum yield of silicon is weak, and normal silicon detectors cannot be used which complicates the measurement. Since a green laser beam excitation will also be absorbed in the silicon, the change of total PL from exciton injection is small, especially for thin singlet fission layers.

Recently, the external quantum efficiency has been used to study the photocurrent contribution from singlet fission materials [29, 76]. If all triplet excitons are utilized for photocurrent, the internal quantum efficiency of the singlet fission materials would be close to 2, which would increase the external quantum efficiency of the silicon solar cell. So far, however, the contributions from triplet excitons could only clearly be distinguished from the noise for very efficient transfer of triplet excitons [29]. The noise level and therefore the error is comparably high because the method relies on accurate optical modeling of the full solar cell stack and the comparison with a reference cell. Again, this method also requires solar cell fabrication, which adds fabrication complications and additional potential for errors.

A necessary requirement for the transfer of triplet exciton energy or charge is the quenching of the triplet exciton at the organic/silicon interface. This effect was used to study exciton transfer by Piland and co-workers [95]. They deposited tetracene layers of varying thicknesses, with and without an insulating spacer layer. They used quenching of the

delayed luminescence lifetime to detect any transfer of triplet excitons at the tetracene/silicon interface. Again, no clear sign of transfer was detected. This method relies on a material that shows delayed fluorescence, originating from the recombination of two triplet excitons into an emissive singlet exciton. It also requires separate samples for each thickness, and is a bulk method, without spatial resolution, while tetracene forms an intricate microstructure [83] which influences singlet fission rates [5].

Here we measure the quenching of the delayed fluorescence with high spatial resolution on a silicon sample covered in many single-crystal tetracene islands of different thickness. We therefore can measure the lifetime quenching for hundreds of different thicknesses in a single measurement on a single sample under the very same conditions (deposition, interface, light excitation and collection). We use this rapid and accurate method to study triplet transfer on tetracene/silicon samples with different interfacial surface treatments, and compare the result to a model of exciton diffusion and transfer. Despite very thin interfacial layers on silicon, and comparable passivation across surface treatments, we find no evidence for transfer of either charge or excitons into silicon. We speculate about the possible reasons and suggest a path towards efficient transfer.

4.2 RESULTS AND DISCUSSION

4.2.1 Quenching on the Interface as a Function of Thickness

A necessary requirement for triplet energy transfer is the change in the delayed fluorescence as a function of distance to the interface. The photoluminescence of singlet fission materials such as tetracene commonly shows two decay components in the polycrystalline thin films, prompt and delayed fluorescence [11]. The prompt fluorescence is due to the quenching of singlet exciton recombination by singlet fission, while the delayed fluorescence stems from the recombination of two triplet excitons to form an emissive singlet state. If the triplet excitons transfer across the interface, then the excitons that experience the interface during their lifetime are quenched (Figure 4.2). Thus, for efficient triplet (singlet)

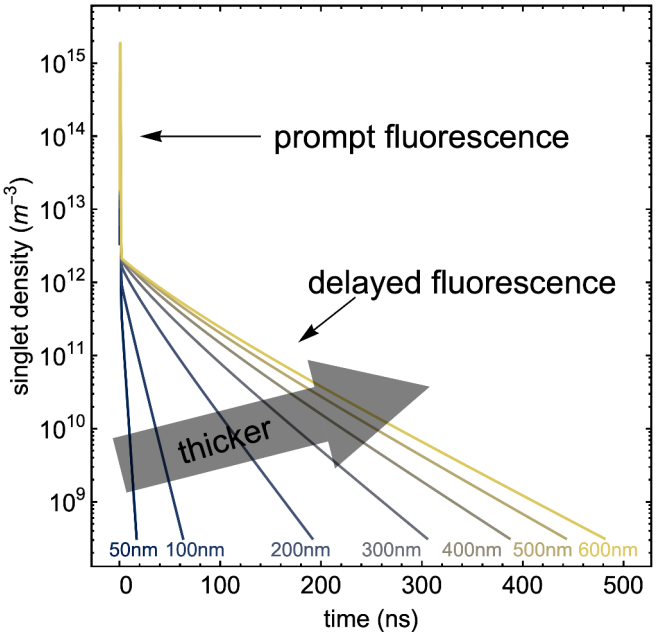

Figure 4.2: Simulation of the singlet density (proportional to the PL intensity) as a function of time. Different colors represent different thicknesses of the tetracene slab. The delayed fluorescence slows down with thicker tetracene layers.

transfer, thinner films will show a shorter delayed (prompt) fluorescence compared to thicker films [95].

To simulate the effect of surface quenching on the photoluminescence we modeled the generation, diffusion and extinction of singlet and triplet excitons. The singlet exciton density profile follows the absorption in tetracene, described by the Beer-Lambert law. Interference effects only have a small effect on the absorption profile, as shown by transfer matrix modeling in the Appendix. We follow Piland et al. [95] to model the generation and recombination of singlet and triplet excitons and add a 1D-diffusion term for singlet and triplet excitons. The quenching (e.g. by transfer into silicon) of triplet excitons is modeled *via* different boundary conditions at the tetracene silicon interface. We initially assume full

quenching but the model also allows to use different quenching efficiencies (surface recombination velocities), as described in the Appendix. The photoluminescence intensity is proportional to the singlet exciton density, which allows us to predict the photoluminescence transients for tetracene islands with different thicknesses. The model shows how the delayed lifetime depends on the film thickness when assuming perfect transfer (Figure 4.2). The model is described by the following differential equations for singlet density (S) and triplet density (T):

$$\frac{\partial S(z,t)}{\partial t} = -k_{SD} S(z,t) + k_{TS} T(z,t)^2 + \\ + excitation(t)\, e^{-\frac{z}{z_0}} + Diff_S \frac{\partial^2 S(z,t)}{\partial z^2}$$

$$\frac{\partial T(z,t)}{\partial t} = -k_{TD} T(z,t) - k_{TS} T(z,t)^2 - k_{TT} T(z,t)^2 \\ + (k_{ISC} + 2k_{fiss})\, S(z,t) + Diff_T \frac{\partial^2 T(z,t)}{\partial z^2}$$

The rates k_{SD} and k_{TD} are the sum of all singlet and triplet decay mechanisms respectively, k_{TS} the triplet to singlet decay rate. $excitation(t)$ is the excitation laser profile with time, multiplied with the exponential decrease of the light intensity according to the Beer-Lambert law inside the slab. $Diff_S$and $Diff_T$are the average diffusion constants for singlets and triplet excitons. k_{TT} is the triplet-triplet annihilation rate. k_{ISC} is the intersystem crossing rate and k_{fiss} is the singlet fission rate. All constants are taken from literature and are shown in the Appendix.

The prompt fluorescence lifetime is only determined by the singlet fission rate, which does not change with tetracene thickness. The delayed fluorescence becomes slower with thicker tetracene layers and levels off after 500 nm (Figure 4.4).

Using our diffusion model, we find that the delayed lifetime should in fact depend on the distance to the interface, while the prompt fluorescence lifetime should be independent of that distance (Figure 4.11 in

Appendix). Note that the length-scales involved here are shorter than the length-scales at which we expect a change in optical coupling into the Si from the refractive index difference and Purcell enhancement of the lifetime because of an enhanced local optical density of states close to a semiconductor interface.

Tetracene, the prototypical singlet fission material, grows in islands on the silicon surface for nominally thin films. These presumably single-crystal islands show a range of thicknesses and can hence be used to distinguish the change in delayed lifetime for a range of distances to the surface. We note that when observing a large area of different islands, any effect of different island heights will be averaged out. Thus, here we probe the lifetime of the islands individually by microscopically-resolved photoluminescence lifetime, and correlate the delayed lifetime of each island to its height. It has been shown that morphology has an influence on singlet fission efficiency [31, 93] and that the growth mode of tetracene changes from 3D to 2D growth with increasing deposition rates above a few Å/s [83]. The tetracene islands in this experiment are grown with a deposition rate of 1 Å/s for all samples, so we can assume that the growth mode stays constant between islands and between samples.

A well-performing silicon solar cell needs a good surface passivation, usually accomplished by amorphous silicon layers, highly doped layers or SiN_x passivation layers. All these layers do not allow for free access to the front side of the silicon that is necessary for direct energy transfer from tetracene into silicon. The close distance needed between tetracene and silicon precludes a thick passivation layer, we therefore probe the transfer on thinner passivating layers. One such passivating interlayer is a short organic molecule that is covalently bound the top layer of silicon atoms. It has been shown that such organic passivation layers can reach a surface recombination velocity comparable to that of good inorganic passivation layers [116]. This layer of organic molecules can also prevent the growth of a native oxide layer between tetracene and silicon. In addition to the passivation and close distance to the surface, the organic molecules could also be used to control the tetracene growth, and therefore its orientation. The orientation of the tetracene molecules on the silicon surface determines the degree of wavefunction overlap

between the triplet exciton and silicon; a larger wavefunction overlap integral leads to a more efficient exciton transfer.

The alignment of the tetracene molecules at the surface depends both on the deposition conditions and on the surface energies, which can be tuned with different capping layers of the organic passivation. We have attached molecules consisting of four benzene rings (pyrene) as interlayers, designed to facilitate the transfer of triplet excitons, and we compare them to our reference sample of thin 2.4 nm thermally grown layers of silicon oxide, which will block the short range (< 1 nm [88]) Dexter type transfer. The Appendix contains the details of the surface modification procedure of aromatic alkynes (phenyl acetylene, 2-ethynylnaphtalene, 1-ethynylpyrene) on hydrogen terminated silicon surface and their characterization. We use ellipsometry and XPS to measure their thickness to be between 1 nm and 1.4 nm; water contact angles to assess their quality and AFM to measure film roughness (see Appendix).

4.2.2 AFM and TCSPC overlay

To measure the delayed fluorescence lifetime as a function of island height, we mark a spot on our substrate and measure both the height of the islands using AFM, and the lifetime using time-correlated single photon counting (TCSPC) microscopy. We then use an automated algorithm overlap the measurements, find the individual islands, and compare the height and lifetime of each of the islands (Figure 4.3)

We combine all pixels that make up an island in the TCPSC data to calculate the lifetime average over that island. From the AFM data of each island we choose to use the mean of the highest 25 % of pixels as a measure for the height of an island. Using the mean of all pixels yields similar results (see Figure 4.16 in Appendix).

Fitting the TCSPC data of the PL decay presents a unique set of challenges. We measure the islands microscopically, therefore we only collect few counts in the delayed fluorescence decay, on the order of 100 photons per island in total. The decay is not mono-exponential, a fact we can already see in our model and the raw decay trace data. We found that

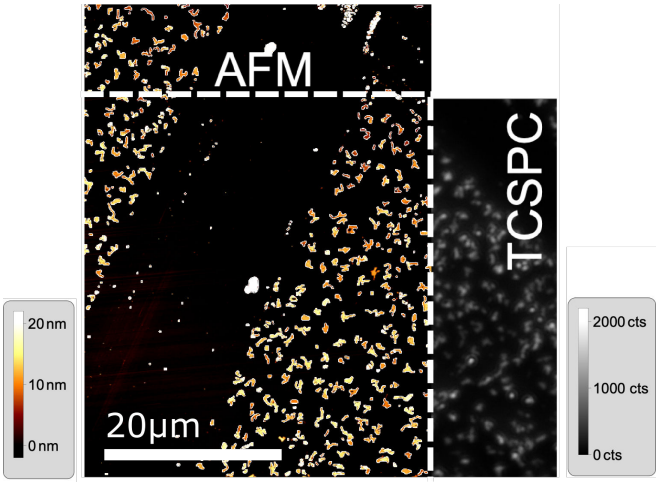

Figure 4.3: Visualization of algorithm that overlays AFM and TCSPC data and identifies islands in both data sets.

the proper accounting of the Poissonian distribution of photons in the low count regime and the choice of a simple fitting model are critical to extract the correct correlation between lifetime and height. Fitting the decay traces with an unsuitable method, for example assuming Gaussian noise, can lead to correlations that are an artifact of the assumption and not the data. More insight into the lifetime fitting and a link to our fitting script can be found in the Appendix.

4.2.3 Comparing the diffusion model with two surface functionalizations

Plotting the delayed lifetime of each island against the height of each island allows us to detect correlations between the two. If there was efficient transfer of triplet excitons, we would expect longer delayed lifetimes at large islands, leading to a positive slope. The results for the samples with oxide grown between the Si and the tetracene are shown in Figure 4.5. The delayed lifetime is related to the slowest timescale fitted, τ_3. For the thermal blocking oxide, we find a slope of $(-3.3 \pm 3.8) \cdot 10^{-2} \frac{\mathrm{ns}}{\mathrm{nm}}$. The pyrene passivation in Figure 4.6 shows a slope of $(-3 \pm 2) \cdot$

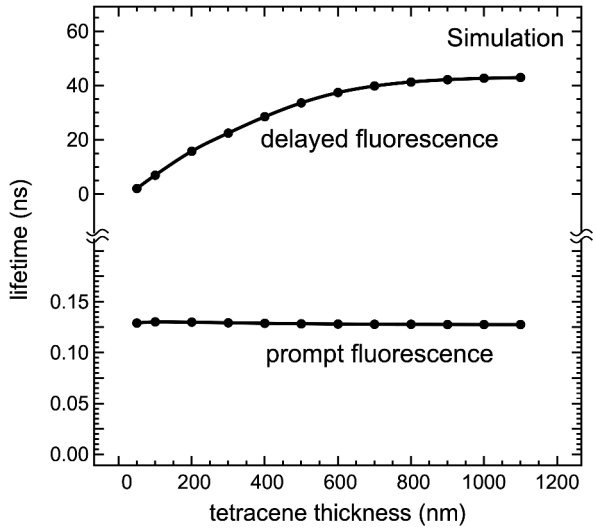

Figure 4.4: Simulation of the lifetimes of a tetracene slab on top of a quenching silicon surface. The values are extracted from Figure 4.2 with a double exponential fit. The delayed fluorescence describes the triplet lifetime and can be used to identify a quenching surface. After a certain thickness the quenching surface does not influence the triplets anymore and the lifetime levels off. The prompt fluorescence is not affected by the quenching surface and stays constant.

$10^{-2}\,\frac{\mathrm{ns}}{\mathrm{nm}}$, both compatible with the absence of any correlation between island height and delayed fluorescence lifetime. The absence of a slope with the pyrene surface passivation techniques in Figure 4.6 shows that there is either no or only very inefficient transfer of triplet excitons.

Different silicon treatments can lead to different tetracene growth modes and interface trap densities which could affect the triplet lifetime. However, the tetracene islands of one sample experience the same surface and environment, which allows us to compare these islands and observe quenching for each surface.

The model we have described above allows us to simulate different quenching efficiencies, from the simulations we can estimate that the

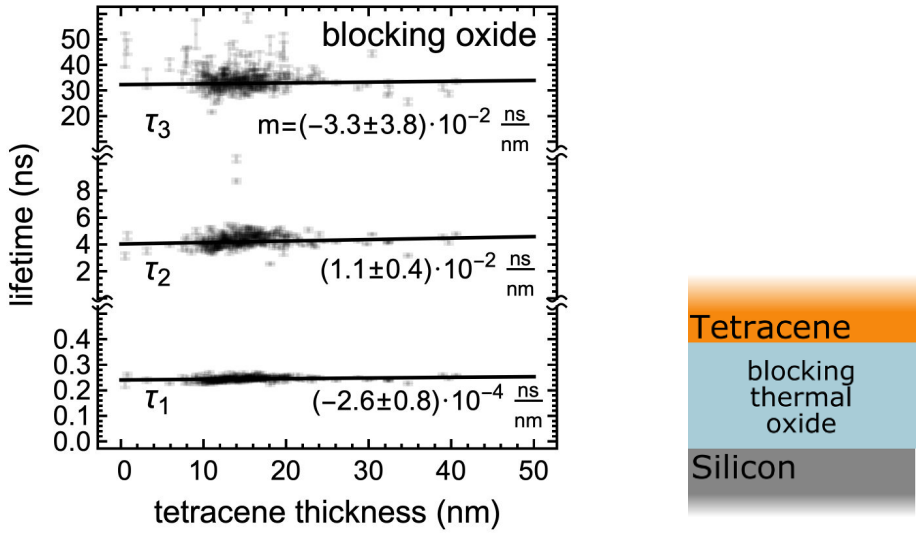

Figure 4.5: The results of the lifetime fitting for the blocking thermal oxide layer. Each data point represents one island. All three exponential functions needed to fit the data do not show a slope within the error, which excludes quenching effects at the interface.

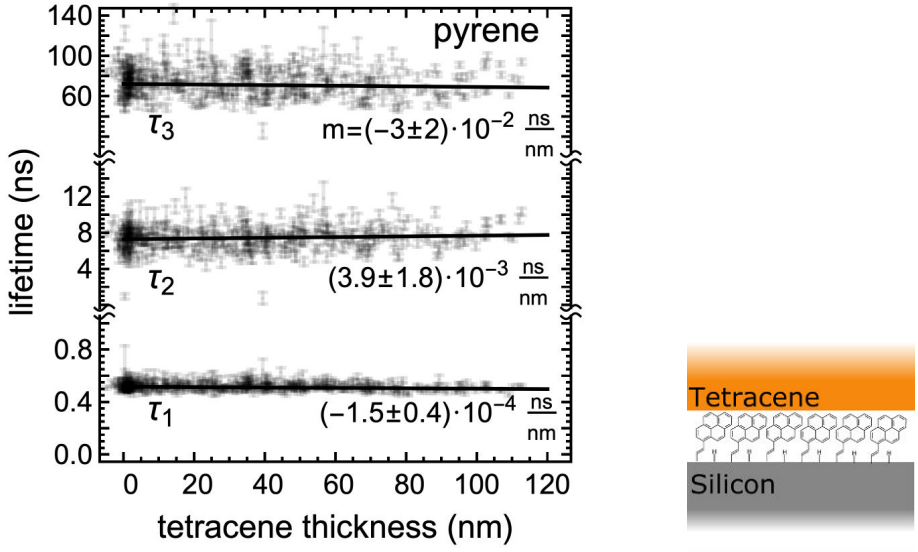

Figure 4.6: Lifetimes of islands on the pyrene treated silicon surface. All three lifetime components show no slope so they are in agreement with no quenching at the surface.

surface quenching in these samples is smaller than 20 $^{cm}/_{s}$ (Figure 4.13 in the Appendix).

We note that our method cannot distinguish between the presence of quenching at the interface by triplet transfer and quenching by charge transfer, surface traps etc.. There are large differences in the silicon surface treatments and presumably trap state density. We measured the surface recombination velocity for all the surface passivation methods described above to study the influence of trapping on triplet exciton lifetime. We find no significant difference in the recombination velocity between samples. This measurement suggests that the triplets are reflected at the interface for all surface treatments, independent of any differences in trap state density.

4.3 CONCLUSION

Any transfer of excitons would lead to a difference in recombination velocity, independent of the transfer mechanism. Therefore, our method cannot be used to distinguish between different mechanisms. However, the mechanism for triplet exciton transfer must be charge transfer or Dexter transfer, because Förster transfer is spin-forbidden. Dexter transfer is the correlated transfer of two electrons where an excited-state electron from the donor transfers into the excited state of the acceptor, and a ground-state electron from the acceptor transfers into the ground state of the donor. Alternatively, the triplet excitons could be quenched by the transfer of just one charge. Any charge transfer, including Dexter energy transfer requires the overlap of the triplet exciton wavefunction of tetracene with the acceptor wavefunction in silicon. Wavefunctions in excitonic materials typically attenuate exponentially with distance, so that close proximity between donor and acceptor is important. All our surface passivation layers are very thin ($\sim 1\,nm$), ensuring close contact between tetracene and silicon. Another important requirement for efficient transfer is the alignment of the triplet exciton wavefunction in relation to the silicon surface. The triplet exciton in tetracene is formed

mostly by the pi-orbitals, which reside on the face of the molecule. Thus, overlap of these wavefunctions would be most efficiently facilitated by horizontal growth where the long axis of the molecule is perpendicular to the silicon interface. We do not have a direct measurement of alignment of the first tetracene molecules on the silicon surface. Different surface passivation layers likely have different formation energies, leading to different alignments of the first crucial tetracene molecules, however we observe absence of quenching in all cases, indicating absence of wavefunction overlap. We note that the exciton wavefunction on tetracene is very localized [6] (the triplet exciton wavefunction has a theoretically calculated root mean square size of 0.35nm [97], experimentally measured to be 0.38 nm [6]) and therefore different in nature from the delocalized Bloch-waves that form the silicon band structure. This difference might introduce additional inefficiencies into the transformation process between the two.

The energy of the triplet exciton (1.25 eV) is larger than the silicon bandgap (1.1 eV) but this is not the only requirement for triplet exciton transfer; the energy levels of triplet exciton in tetracene and the bands in silicon have to align with respect to vacuum. This alignment should be fulfilled in HF-etched silicon [76] but they may misalign with our different surface passivation layers.

Since any of the bottlenecks discussed above can block the transfer of energy, it is important to develop microscopic models and measurements to investigate the rich physical system of the organic-inorganic interface. In this paper we have described a method for sensitive quenching detection at an interface between tetracene and silicon by only using a TCSPC lifetime map and AFM height data. Correlating the delayed fluorescence and the thickness of islands with different heights allows us to detect quenching of triplet excitons. Quenching is the necessary requirement for triplet exciton transfer, which would be technologically interesting for applications in singlet fission solar cells.

APPENDIX

SAMPLE FABRICATION

Aromatic Monolayer Formation

Hydrogen terminated surface preparation

1 × 1 cm pieces of n-Si (111) were consecutively sonicated for 10 minutes in: acetone, ethanol and DCM. Subsequently the wafers were dried by a stream of argon and placed in Harrick plasma cleaner connected to a Harrick PlasmaFlo for plasma treatment. Followed by a purging of the chamber with Argon for 5 minutes. After 10 minutes of plasma treatment the samples were swiftly transported into a Nitrogen filled glovebox, where upon the samples were placed in an Argon saturated 40 % ammonium fluoride solution, to etch for 15 minutes. Next, the etched samples were rinsed with argon-saturated milli-Q-water and blown dry by a stream of argon [101].

Surface Modification Aromatics

The freshly etched and rinsed surfaces were then submerged in 2 mL neat phenyl acetylene or a 20 % v/v mesitylene (in case of 2-ethtnyl naphthalene and 1-ethynyl-pyrene) solution of the desired solution which had been placed under high vacuum (10 mbar) for at least 1 h prior to submergence. The submerged samples were then kept at 80 °C overnight as was described in previous surface modification literature [116] after which the surfaces were washed with DCM within the glovebox and prior to storage again sonicated for 10 min in DCM.

Monolayer Characterization

Static Contact Angle (SCA): Static water angle measurements were made with an automated Krüss DSA 100 goniometer. Depending on the size of the modified surfaces 2-3 droplets were dispensed on the surface and the contact angles were determined using a Tangent 2 fitting model. The standard error in the determined contact angles is approximately 1°.

Ellipsometry

The elipsometric thicknesses of the samples were assessed by using a Sentech Instruments type SE-400 ellipsometer, operating at 623.8 nm (He-Ne laser), and an angle of incidence of 70°. The optical constants of a freshly etched hydrogen-terminated Si(111) surface were taken as $n = 3.821$ and $k = 0.057$. The reported values are the result of a planar three layered (ambient, monolayer, substrate) model with the assumed refractive indices of 1.00 and 1.46 for the ambient and monolayer respectively. All the reported values are averages of at least 10 measurements and the error is approximately 0.2 nm.

X-ray Photoelectron Spectroscopy (XPS)

X-ray photoelectron spectroscopy (XPS) spectra were attained on a JPS-9200 photoelectron spectrometer (JEOL,Japan). The analysis was performed under ultra-high vacuum conditions using a monochromatic $Al\,K-\alpha$ X-rays $(h\nu = 1486.7eV)$ at 12 kV and 20 mA and an analyzer pass energy of 10 eV. A take-off angle φ of 80° was used. All the XPS spectra were processed with Casa XPS software (2.3.18) and the binding energies were calibrated on the hydrocarbon (CH_2) peak with a binding energy of285.0 eV.

Atomic Force Microscopy (AFM) of aromatic monolayers

Atomic Force Microscopy measurements were obtained by means of an Asylum MFP-3D Atomic Force Microscope which was equipped with a 100-micron closed-loop XY-stage which allows for AFM imaging as well as precise sample positioning. A minimum of two scans per modified surface at 20 x 20, 5 x 5 and 1 x 1 μm were made in standard ACAirTopography mode. After the measurements, a height and roughness profile was produced using the AFM Analysis tool in Igor Pro 6 with a third order flattening.

Interlayer Characterization

In this section we will be further discussing the obtained results of the various aromatic organic monolayers on Si(111). The polyacene like monolayers are also referred to as the aromatic surfaces.

Silicon functionalized with aromatic surfaces

All the aromatic functionalized silicon surfaces summarized in Figure 4.7: silicon modified with phenylacetylene (Si-Ph) and silicon modified with 2-ethynyl-napthalene(Si-Naph), silicon modified with 1-ethynyl pyrene (Si-Pyr), silicon modified with 1-ethynyl pyrene and backfilled with 1-pentyne and respectively all three aromatic surfaces covered with a layer of tetracene (Si-Ar-tetracene) are all functionalized with two aims in mind. First, to prevent the oxidation of hydrogen-terminated silicon and second to enable or enhance the previously explained Dexter energy transfer into the silicon bulk. The following paragraphs will further elaborate as to how these aromatic monolayers were characterized.

Characterization of the aromatic surfaces

After the aforementioned sample preparation and modification and prior to any characterization, three samples of each batch were measured by ellipsometry for a first indication of the quality of the desired monolayer.

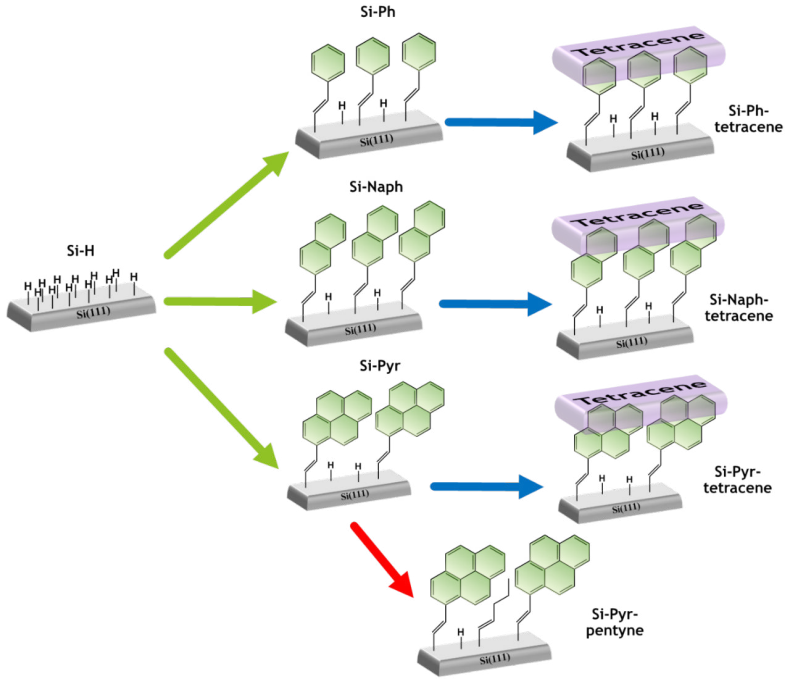

Figure 4.7: Overview of the different modifications of the various aromatic surfaces. First Si-H is modified with different SAMs to either Si-Ph, Si-Naph or Si-Pyr. These surfaces then have 4-40 nm tetracene deposited onto them resulting in Si-Ph-tetracene, Si-Naph-tetracene and Si-Pyr-tetracene. Alternatively, to prevent the rapid oxidation of Si-Pyr one can backfill surfaces with pentyne to counteract immediate oxidation resulting in Si-Pyr-pentyne for example.

Mono layer	Theoretical (Chem 3D, Å)	Measured (Ellip, Å) (±2 Å)	C:Si (XPS, %) (±2 %)	Measured (XPS, Å) (±2 Å)
Phenyl acetylene	6.5	10	23.3:75.5	9.2
2-ethynyl naphtal.	8.5	12	25.9:68.0	11.0
1-ethynyl pyrene	10.6	14	28.5/71.5	14.5

Table 4.1: Overview over the different heights per surface. The theoretical column is found measuring the differences of the top and bottom carbon in Chem3D, the measured column represents the averages of ellipsometry measurements, the C:Si ratio is obtained by the XPS wide scans and lastly the calculated column logically follows from using the previously found C:Si ratio in Equation 1.

The theoretical length of the monomer was assessed by using a model of the completely stretched out monomer in Chem3D. This would give an adequate upper-limit to what a completely sterile modified surface would look like. Table 4.1 accordingly summarizes the findings across several batches and several surfaces, note that the reported values are averages of all the measurements. Additionally, the thickness of the layer was also calculated by means of using the carbon: silicon ratio supplied by the XPS wide scans and the following equation:

$$Th_{xps} = \lambda_M^{Si} \sin(\varphi) \ln\left(1 + \frac{C}{Si}\right)$$

with $\lambda_M^{Si} = 38.5\text{Å}$ and $\varphi = 80°$, where Th_{xps} represents the thickness from using the C:Si ratio found by the XPS wide-scan, λ_M^{Si} being the attenuation length of the Si 2p photoelectron and φ representing the angle between the surface plane and the detector.

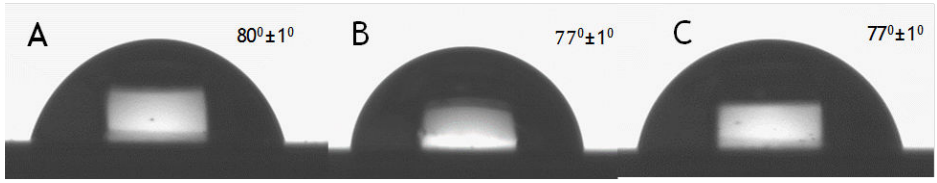

Figure 4.8: A) Snapshot of Si-Ph surface with a Mili-Q-water droplet with an SCA angle of 80°. B) A picture of Si-Naph with a Mili-Q-water droplet with an accordingly SCA of 77° and lastly C) is the same as A and B but now with a Si-Pyr surface also with a SCA of 77°.

Interestingly, both the measured and calculated heights of the functionalized surfaces exceed the theoretical upper limit of the completely stretched out molecule. The differences between the measured and theoretical values may be due to the uncertainty associated with the ellipsometry measurements (index of refraction, cleanliness of the silicon etc.) [3, 127]; however, Jakubowicz et al. have similar ellipsometric data when comparing p-nitrobenzenethiol monolayers on gold surfaces [54]. The ellipsometry data here can only serve as a qualitative support of the "monolayer" nature of the adsorbed film and thus the interpretation should be regarded with some degree of reservation until more evidence is available. Nonetheless, several anstrom differences by ellipsometry and an overestimation based on the carbon to silicon ratio by XPS also seem to point that there is some physio-absorption. To counter this the surfaces post modification are sonicated in DCM and toluene but the heights still exceed the upper limit found by Chem3D.

After checking the initial quality of the batch several other experiments were conducted to further assess the quality of the aromatic surfaces. Amongst these tests is the static water contact angle. On every surface a minimum of three drops were placed and for all three surfaces a minimum of two different batches were measured. Comparing the SCA findings (Figure 4.8) to those previously reported[3, 63] for Si-Ph it becomes apparent that the static contact angles are smaller than reported by Kondo et al.[63]. This difference could either be attributed to local impurities or a not perfectly homogeneous monolayer. Additionally, the

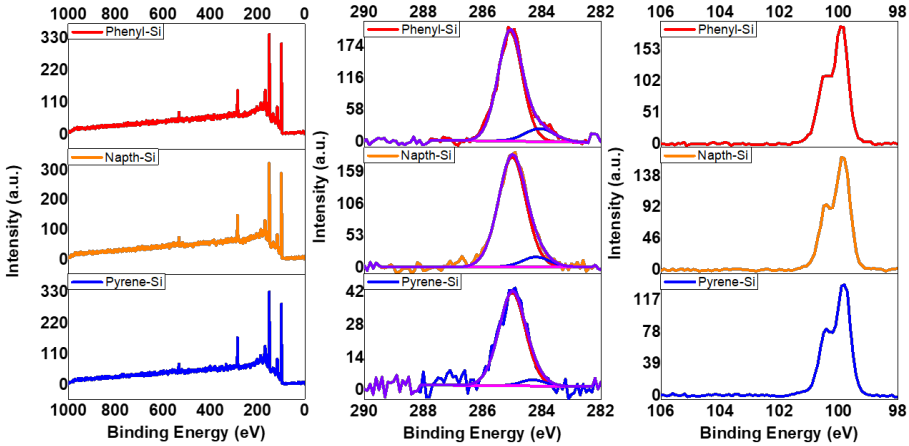

Figure 4.9: XPS data of different surfaces. Top row is the wide scan, the carbon narrow scan and the silicon narrow scan of a Si-Ph surface. Middle row is the wide scan, the carbon narrow scan and the silicon narrow scan of a Si-Naph surface. Bottom row is the wide scan, the carbon narrow scan and the silicon narrow scan of a Si-Pyr surface.

difference in SCA between Si-Ph, Si-Naph and Si-Pyr is hypothesized to be due to the lower density of these SAMs. These surfaces would more readily oxidize and therefore also show lower SCA values.

Having completed a first assessment of the various aromatic functionalized silicon surfaces, to either deem a batch successful or not, two samples were submitted for further XPS analysis. Figure 4.9gives an overview of the carbon and silicon narrow scans of Si-Ph, Si-Naph and Si-Pyr. In the Si narrow scans the emission peaks of 99.5 eV and 100.1 eV correspond to the $Si2p_{3/2}$ and $Si2p_{1/2}$ respectively (see Figure 4.9 right side column). More importantly a flat baseline around 103 eV is present in all surfaces; this is indicative of the absence of a silicon oxide (SiO_x) layer. This is of vital importance to the overall functioning of the proposed cascade outlined in the theory section as the oxide would act as a pacifying layer and thus the absence of it is key. Additionally, the absence of any other distinguishable peaks aside from the characteristic C-C peak (285 eV) in

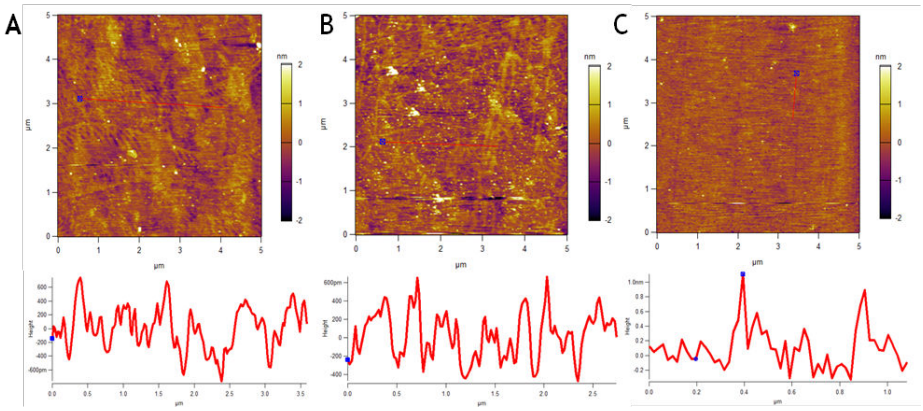

Figure 4.10: AFM and height profiles of A) Si-Ph (RMS = 0.4 ±0.2 nm), Si-Naph (RMS= 0.5 ±0.2 nm) and Si-Pyr (RMS= 0.3 ±0.2 nm)

the carbon narrow scan is a good indication that no carbons are bound to other heterogeneous elements (see Figure 4.9, middle column) and at 284 eV which corresponds to the Si-C=C- peak.

Lastly, AFM measurements were taken of a minimum of two surfaces at (at least) two different spots on the respective surface. Figure 4.10 shows the 5 µm areas of the Si-Ph, Si-Naph and the Si-Pyr modified surfaces, below each respective surface are profile plots to give an indication of the roughness of the surface. In the case of Si-Ph the upper and lower limit vary between −400 to600 pm or approximately 1 nm. Similarly, for Si-Naph the upper and lower limit are between −300 to 600 pm, and lastly with Si-Pyr the limits range from approximately −0.1 nm to 1 nm. The respective RMS values are 0.4,0.5 and 0.3 ± 0.2 nm for Si-Ph, Si-Naph and Si-Pyr respectively.

Together, the acquired data suggests that various aromatic surfaces were modified successfully and are oxygen free. The thicknesses range from $9 - 16$ Å which is within the typical Dexter Energy transfer range of $6 - 20$ Å. Similar results were obtained by Garg et al.[35] especially with respect to the SCA, ellipsometry and 1×1 µm AFM measurements. The key difference is that in their research they were modifying hydrogen-

terminated silicon with longer alkyl chains whereas in this research exclusively ethynyl substituted polyacenes were used.

Thermal blocking oxide

For the samples with a thermal blocking oxide the silicon wafer was first HF etched (2 % HF aquous solution) for 3 minutes to remove the native oxide. The samples were then transferred into a rapid thermal annealing chamber and were heated under constant nitrogen flow of 1 l/min to 775 °C and kept at that temperature for 10 s under an O_2 flow of 1.5 l/min. The resulting SiO_2 film thickness was characterized with Ellipsometry to be 1.9 nm and XPS to be 2.4 nm following Lu et al. [74].

Tetracene evaporation

Sample Preparation: Tetracene was evaporated inside an Angstrom Engineering thermal evaporation chamber at room temperature below 7×10^{-7} mbar. Tetracene was bought from Sigma-Aldrich in 99.99 % purity and used as is. The nominal evaporation thickness was 2 nm at an evaporation speed of 1 Å/s. The samples were encapsulated in nitrogen atmosphere using two glass slides and a rubber gasket. We use a sharp needle to scratch a cross into the tetracene layer that serves as a reference to find the same area in the AFM and the TCSPC setup and facilitates the data overlay.

AFM measurement of tetracene islands

AFM was measured with a Bruker Instruments Dimension Icon atomic force microscope in PeakForce tapping mode with Scan Asyst.

TCPSC measurement

We performed all experiments in a home built TCPSC setup, using a PicoQuant LDH-D-C 485 nm laser, fiber coupled into a Nikon 60x water immersion objective (PlanAPO VC 60x A/1.2 WI). The same objective is collecting the photoluminescence. The excitation light is filtered with a 488 nm notch filter and a 500 nm longpass filter in the detection path. The detectors used are silicon-single photon avalanche detectors (Micro Photon Devices, MPD-5CTD). The detectors are connected to a PicoQuant HydraHarp 400 event timer with a repetition rate of 0.7 MHz. The TCPSC lifetime map is created by scanning a PI piezo stage. Control of the laser, piezo stage and detectors is handled by PicoQuant SymphoTime software. The average excitation density over time is estimated to be $80\frac{W}{cm^2}$.

DIFFUSION MODEL

The Diffusion model uses the model of Piland et al. [95] as a starting point and. Piland and coworkers use a coupled differential rate equation for the density of singlets and triplets over time. We then add the 1D diffusion of both triplet and singlet excitons to the differential equation by using Fick's second law, resulting in the equations used in the main text.

The excitation source is modeled as a normal function with a variance of 150 ps which is also a realistic value for our experiment. The excitation function is also visible in light blue in Figure 4.11. We solve the differential equations for each time after the initial excitation.

The following constants have been used: $\mathrm{Diff_S} = 2.8\mathrm{cm^2/s}$ and $\mathrm{Diff_T} = 0.0023\mathrm{cm^2/s}$ taken from Wan et al. [137]. $\mathrm{kRad} = 8 \times 10^7\,1/\mathrm{s}$, $k_{IC} = 0$, $k_{ISC} = 0$, $k_{fiss} = 8.3 \times 10^9\,1/\mathrm{s}$, $k_{ee} = 1 \times 10^{-8}\mathrm{cm^3/s}$,

$k_{SD} = k_{RadS} + k_{IC} + k_{ISC} + k_{fiss} + k_{ee}$, $\mathrm{kTriplet} = 6.7 \times 10^6\,1/\mathrm{s}$, $\mathrm{kTS} = 0.5 \times 10^{-10}\mathrm{cm^3/s}$, $\mathrm{kTT} = 2 \times 10^{-10}\mathrm{cm^3/s}$, and $\mathrm{Excitation} = 30 \times 10^3\,\mu\mathrm{m}^{-3}$.

The boundary conditions for the singlet exciton density are as follows: $S(z, t = 0) = 0$ meaning there are no singlet excitons present before excitation. At the interface $\frac{dS(z,t)}{dz} = 0$ at $z = 0$, so that there is no flux of

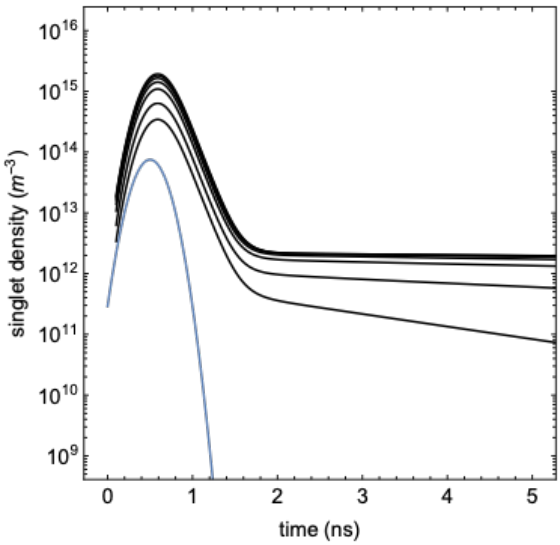

Figure 4.11: Simulation of Singlet decay upon excitation pulse (light blue) for different thicknesses of tetracene. The prompt fluorescence is not affected by the thickness. The blue curve indicates the excitation rate (in $m^{-3}ns^{-1}$).

singlets at the boundary of tetracene and silicon. The flux at the top of the tetracene slab is also set to zero (at z = thickness).

The boundary conditions for the triplet excitons are set so that there are no triplet excitons at time zero. At the top of the tetracene there is no outward flux of triplet excitons, just as with the singlet excitons. A crucial difference between singlet and triplet excitons in our model is the behavior at the tetracene-silicon interface, for triplets we set the density to zero at all times, which simulates perfect quenching at this interface.

We can also simulate a different quenching efficiency of the triplets in tetracene for a wide range of thicknesses. We implement this by replacing the boundary condition at the interface between tetracene and silicon. Before the triplet exciton density was set to zero at the interface - a perfect quenching scenario. Now we set the density the interface to a quenching rate which is the y-axis in Figure 4.12. From this plot it

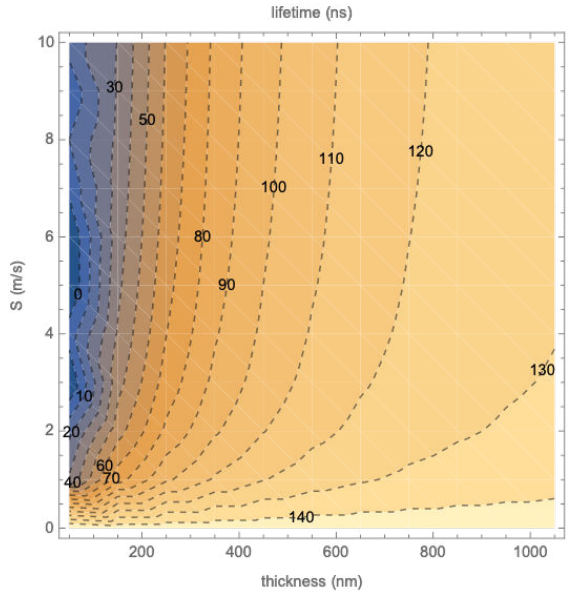

Figure 4.12: Plot of the delayed fluorescence as a function of the quenching speed, expressed in a surface recombination rate (m/s). The numbers in the plot are the delayed fluorescence lifetimes, with their corresponding contour lines. The quenching rate levels off for higher quenching rates.

becomes evident that below a certain quenching rate, here represented by a surface recombination velocity of 1 m/s, the lifetime change with thickness becomes shallower. This would mean that it would be harder to detect in the experiment, and the trend is also not linear any more.

We can use this plot to estimate a lower bound for the quenching rate that we observe in our experiment. A crosscut along Figure 4.12 in the horizontal axis (S, quenching rate) and for low quenching rates < 1 m/s shows at which quenching rates we should expect a slope of delayed lifetime vs thickness in our experiment. Even at 20 cm/s there is a significant slope, so we can safely conclude that our quenching rate is below 20 cm/s for all surfaces in the experiment.

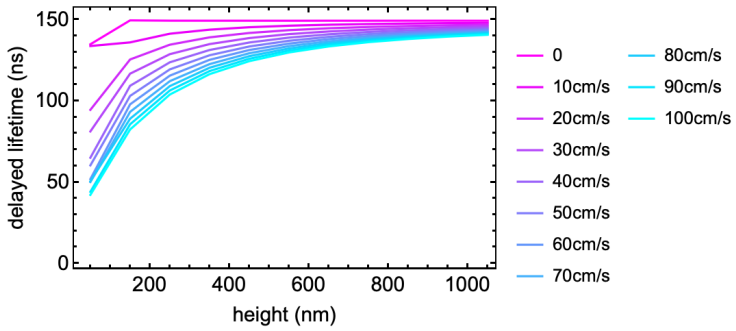

Figure 4.13: Horizontal cross cuts through Figure 4.12 in the low quenching regime for specific quenching rates. Even at 20 cm/s there is still a considerable delayed lifetime slope that should be observable in the experiment.

Transfer Matrix modeling of absorption in tetracene

We calculated the absorption of laser light with a transfer matrix model to investigate whether interference effects influence the absorption modelling in our diffusion model. In the diffusion model the absorption is assumed to follow the Lambert-Beer law.

The software used to perform the transfer matrix simulations is the Python implementation of a transfer matrix model developed at the McGehee group in Stanford [12]. The model assumes that the layers are flat and indefinitely large, which is not necessarily the case in the island structures we have on our samples.

We use the complex refractive index of air, tetracene and crystalline silicon to set up the simulation. The incoming light is a laser beam at 485 nm, orthogonal to the substrate, with a FWHM of 7 nm and a power of 100 mW/cm^2, which corresponds to a current density of 40 mW/cm^2 (assuming an IQE of 100 %).

The absorption in the active material, tetracene, is calculated as a function of the thickness.

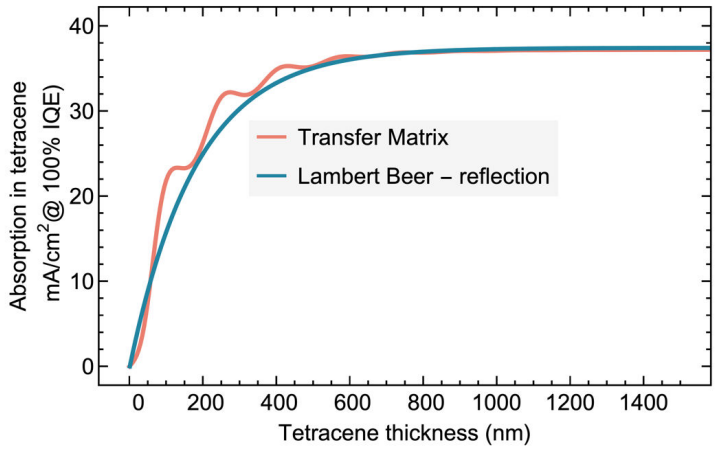

Figure 4.14: Comparison of the Lambert-Beer law of absorption and the transfer matrix calculations. The Lambert-Beer law is corrected for the reflection at the interface between air and tetracene. The oscillations on top of the lambert-beer absorption is due to interference effects included in the transfer matrix model.

Interference effects on the absorption are included in the transfer matrix calculations which leads to oscillations in the absorption as a function of thickness, visible in Figure 4.14.

These are secondary effects are neglected in the diffusion simulation, since the only change is in the initial charge carrier distribution inside the tetracene slab. Small differences here would not result in drastically different triplet distributions, and we have therefore chosen to use the simpler Lambert-Beer profile. For samples where the cavity effects are more severe one might chose to use transfer matrix modeling to determine the initial singlet exciton profile.

In addition to the absorption changes from the cavity effect, the singlet exciton can also change its lifetime close to a reflecting surface (Purcell enhancement [4]). We note, however, that the delayed fluorescence lifetime is determined by the slow triplet-triplet annihilation rate and not the singlet decay rate, so lifetime enhancement effects of a dipole emission

close to a dielectric surface can be neglected if the singlet fission rate is much larger than the singlet exciton emission rate, as is the case in tetracene.

IDENTIFICATION OF ISLANDS

Procedure to identify islands in AFM and TCSCP data: In order to identify the islands in the AFM data we first import the raw AFM data and convert it into a grey scale image. This image as well as the TCSPC image is then converted into a black and white image. Since the background is changing slightly it is important to use a binarization function that only takes the immediate surroundings into account. The binarized image of fore- and background then allows us to dissect each island. The linear transformation between both AFM and TCPSC picture can be used to identify each island that are the same in each dataset. Figure 4.15 shows the quality of the overlap.

HEIGHT DETERMINATION

The height of an island is defined by the mean of the top 25% of pixels. This measure is more robust to outliers than taking the maximum but still representative of the maximum height of the island. Figure 4.16 shows the difference between different ways of measuring the height of a tetracene island for one example island.

FITTING OF TCSPC DATA

By summing up the TCSPC data for each island we can fit the very low intensity PL decay of the delayed fluorescence. Since the delayed fluorescence is several magnitudes less intense than the prompt fluorescence the

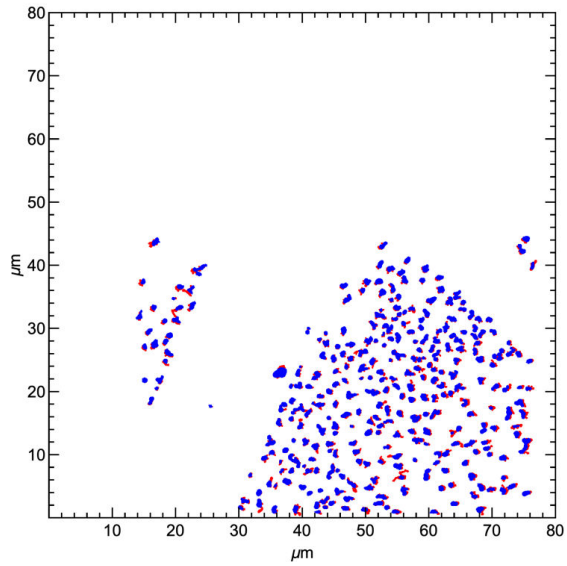

Figure 4.15: Blue is TCSPC and Red is AFM data. The overlay of islands is good, which allows us to compare AFM and TCSPC data on an island to island basis.

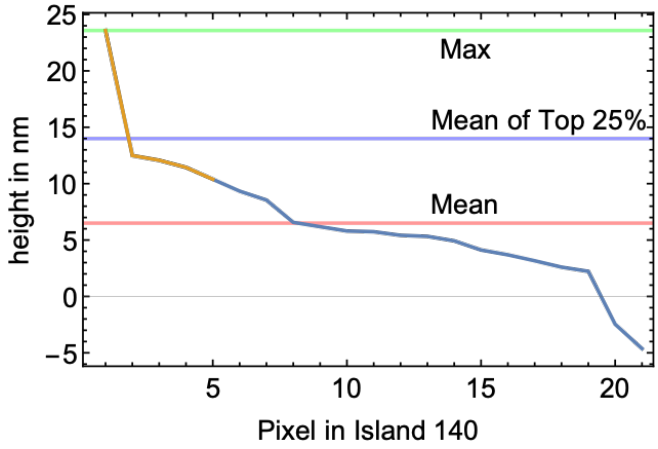

Figure 4.16: All height values of one typical island sorted by height. Green: maximum value. Blue: mean of top 25 %. Red: mean of all pixels. The line in orange are the largest 25 % of the pixels, used to calculate the blue line.

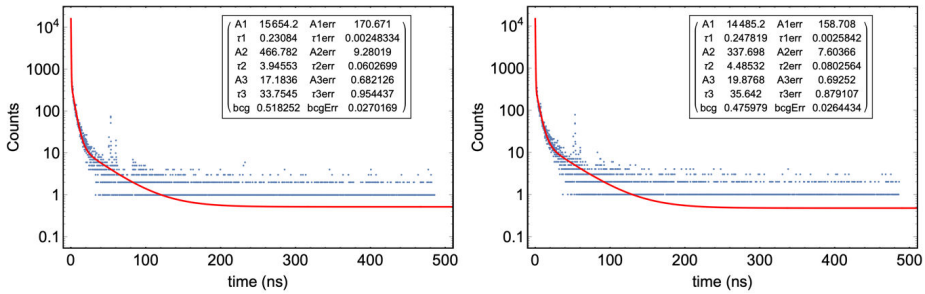

Figure 4.17: Fit of two example islands of the oxide sample for the three-exponential function with the MLE fitting algorithm. Resulting parameter estimates and errors are shown in the inset.

number of photons in the delayed fluorescence is low and each photon is important for the noise level.

We need three exponentials to properly describe the data. One for the prompt fluorescence, one for the intermediate region and one for the delayed fluorescence. This can only be seen as a representation of the data and cannot be used to rationalize an underlying rate-equation model. It is however sufficient to quantify the changes in each lifetime with a change in height.

Since the we only have a few photons in the low intensity region of the PL decay traces, fitting with an algorithm that uses the sum of the least-squares is no longer valid. The least-squares fitting assumes the noise of the data to be distributed like a normal distribution. In our case though the proper noise distribution is poissonian since we count individual photons. In most cases this difference is not important since the normal distribution approximates the poissonian distribution well if the mean is larger than 15. In our experiment the number of photons per bin is regularly below 10, so we cannot use the least squares fit. The proper cost function to minimize to find the best fit is the so-called Maximum-Likelihood-Estimation. With this method we can define the correct Poissonian noise distribution. We have implemented this algorithm in MATHEMATICA 12. Two example fits can be seen in Figure 4.16.

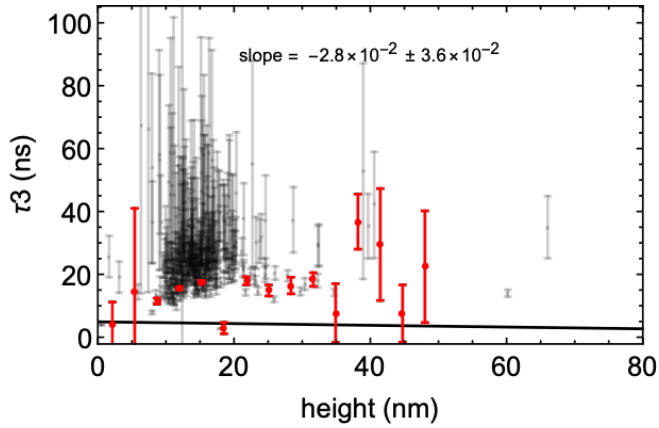

Figure 4.18: Fitting of thermal oxide islands fitted with the standard least-squares algorithm. The error bars are extremely large and the mean value does not correspond with the MLE fitting result. Each grey point represents one tetracene island, the red points are averages of the grey points in a certain height range.

The need for the proper account of the noise can also be seen if we attempt to fit the data with the standard least-squares fitting as implemented in the MATHEMATICA function NonLinearmodelFit. The error bars are much larger and the mean value of the long lifetime is also far from the real value retrieved by the MLE fitting. This is shown in Figure 4.18.

It has also been suggested in literature [95] to only fit the end of the decay with one exponential as a way to measure the delayed fluorescence lifetime. This however is heavily dependent on the starting point of where we fit the data. In Figure 4.19 we can see that the slope of lifetime vs. height we get from the tetracene-oxide sample is positive, negative, or zero depending on the start value of the fit, eg. how many data points are considered to be part of the delayed fluorescence. We therefore deem this fitting procedure unreliable for our dataset.

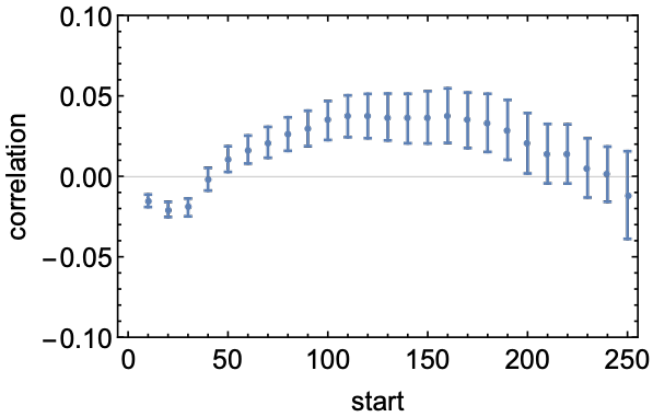

Figure 4.19: Slope of delayed lifetime vs. height for the tetracene-oxide sample as a function of the start value of a mono-exponential fit. The value of the slope and therefore the indication of quenching is highly dependent on the start point.

SURFACE PASSIVATION MEASUREMENT USING PHOTOCONDUCTANCE

Microwave photoconductance decay (μPCD) measurements were performed on a Semilab WT-2000 tool. After illumination of the sample with a 200 ns laser pulse (904 nm, 1.2×10^{12} photons/pulse), photoconductance decay is determined from the reflected microwave intensity (at 10.3 GHz), which is a measure of the free carrier concentration in the sample. The carrier lifetime is then extracted from the recorded transient. Lifetime maps were recorded with a 1 mm^2 laser spot and 125 or 250 μm step size. We can see in Figure 4.20 that the free carrier lifetime does not differ significantly between the different functionalized samples and bare silicon, indicating a poor surface passivation effect of the functionalized samples.

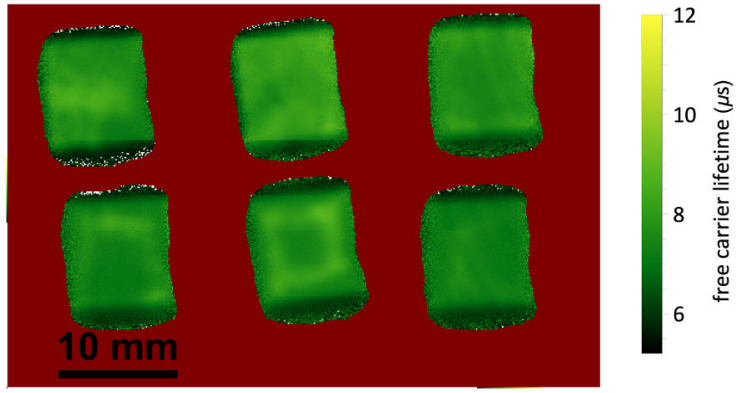

Figure 4.20: Free carrier lifetime in silicon for six different 10x10 mm silicon samples. The top row are the functionalized silicon samples, with Si-Ph, Si-Naph or Si-Pyr from left to right. The bottom row is bare n-doped silicon <111>. We can see that the passivation quality is comparable between all samples.